# On Godunov-Type Lagrangian Methods

Daniel Zaide

August 18, 2009

**NOTE:** I don't in any way claim that all of this work is original, it is simply written to serve as an internal reference and guide to what I'm currently doing.

# 1 Introduction

# 2 Governing Equations

The Euler Equations can be written in Arbitrary Eulerian-Lagrangian form as

$$\mathbf{u}_t + \mathbf{f}^i(\mathbf{u})_{x_i} = 0 \tag{1}$$

or, expanded as

$$\frac{\partial}{\partial t}\begin{bmatrix} \rho \\ \rho\mathbf{v} \\ E \end{bmatrix} + \nabla \cdot \begin{bmatrix} \rho(\mathbf{v}-\dot{\mathbf{x}}) \\ \rho\mathbf{v}(\mathbf{v}-\dot{\mathbf{x}}) + \mathbf{I}p \\ (\mathbf{v}-\dot{\mathbf{x}})(E+p) \end{bmatrix} = \begin{bmatrix} 0 \\ 0 \\ 0 \end{bmatrix}, \tag{2}$$

with the equation of state $p = p(\rho, i)$. For an ideal gas as

$$p = (\gamma-1)\rho i, \qquad \rho i = \left(E - \frac{1}{2}\rho\mathbf{v}^T\mathbf{v}\right) \qquad H = \frac{E+p}{\rho} \tag{3}$$

# 3 Time-Stepping Method

Here, only 1D methods are shown but both methods extend naturally to two or three dimensions.

## 3.1 Hancock

To achieve second-order in space and time, a generalized Hancock-type scheme is used [1]. This method was first described by Berthon [2] and later expanded to third-order by Suzuki, in a Ph.D. Thesis done in 2008 under Bram van Leer [3]. Define the new nodal positions $x_i^{n+1} = x_i^n + \Delta t \dot{x}_i^n$ with an interface speed $\dot{x}_i^n$. By integrating the conservation law (1) around the control volume we obtain

$$\mathbf{u}_i^{n+1}(x_{i+\frac{1}{2}}^{n+1} - x_{i-\frac{1}{2}}^{n+1}) = \mathbf{u}_i^n(x_{i+\frac{1}{2}}^n - x_{i-\frac{1}{2}}^n) - \Delta t\left(\mathbf{f}_{i+\frac{1}{2}} - \mathbf{f}_{i-\frac{1}{2}}\right). \tag{4}$$

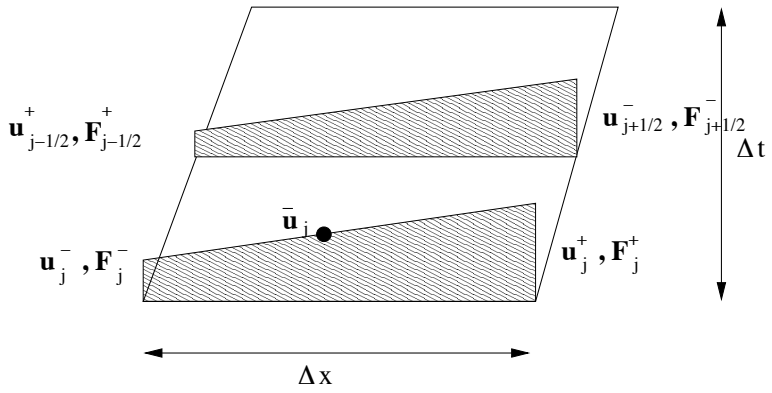


Figure 1: A finite volume cell in a one-dimensional mesh.

In Hancock's method we take the initial data in cell $i$ be

$$\mathbf{u}_i(x,0) = \bar{\mathbf{u}}_i + \tilde{\mathbf{S}}_i(x - \bar{x}_i), \tag{5}$$

where the bar denotes cell averaged values and the slopes $\tilde{\mathbf{S}}_i$ are limited. Evaluate $\mathbf{u}_i$ at the left and right cell edges, giving $\mathbf{u}_i^-$ and $\mathbf{u}_i^+$. From these states, evaluate $\mathbf{f}_i^-$ and $\mathbf{f}_i^+$. Then, halfway through the timestep evaluate

$$\mathbf{u}^+_{i-\frac{1}{2}} = \bar{\mathbf{u}}_i - \tilde{\mathbf{S}}\left(\frac{1}{2}\Delta x_i - \frac{1}{2}\Delta t u_{i-\frac{1}{2}}\right) - \frac{1}{2}\frac{\Delta t}{\Delta x_i}(\mathbf{f}_i^+ - \mathbf{f}_i^-) \tag{6}$$

$$\mathbf{u}^-_{i+\frac{1}{2}} = \bar{\mathbf{u}}_i + \tilde{\mathbf{S}}\left(\frac{1}{2}\Delta x_i + \frac{1}{2}\Delta t u_{i+\frac{1}{2}}\right) - \frac{1}{2}\frac{\Delta t}{\Delta x_i}(\mathbf{f}_i^+ - \mathbf{f}_i^-). \tag{7}$$

These are the states to use in the Riemann problem. It should be noted that using a constant, first-order reconstruction of $\mathbf{u}_i(x) = \overline{\mathbf{u}}_i$ reduces the method to a first-order in space and time Forward Euler. **Note:** In the ALE case, its doesn't matter, but in the Lagrangian case, the fact that the vertex velocity is $u^n$ and the flux is evaluated at $n + \frac{1}{2}$ may lead to the fact that $\mathbf{f} - u\mathbf{u} = \mathbf{f}^{n+\frac{1}{2}} - u^n\mathbf{u}^{n+\frac{1}{2}} = [0, p^{n+\frac{1}{2}}, u^n p^{n+\frac{1}{2}}]^T \neq [0, p^{n+\frac{1}{2}}, u^{n+\frac{1}{2}} p^{n+\frac{1}{2}}]^T$which seems to lack consistency to me. I'm not completely sure about this being a problem, but in the first-order case, it doesn't matter.

## 3.2 Second Order Runge Kutta

First, let

$$\mathcal{R}(\mathbf{u}) = -\left(\mathbf{f}_{i+\frac{1}{2}} - \mathbf{f}_{i-\frac{1}{2}}\right). \tag{8}$$

In the ALE case, we take the first step as

$$x_i^{(1)} = x_i^n + u_i^n \Delta t \tag{9}$$

$$\mathbf{u}_i^{(1)}(x^{(1)}_{i+\frac{1}{2}} - x^{(1)}_{i-\frac{1}{2}}) = \mathbf{u}_i^n(x^n_{i+\frac{1}{2}} - x^n_{i-\frac{1}{2}}) + \Delta t \mathcal{R}(\mathbf{u}^n) \tag{10}$$

The second step is then

$$x_i^{n+1} = \frac{1}{2}x_i^n + \frac{1}{2}x_i^{(1)} + \frac{1}{2}u_i^{(1)}\Delta t \tag{11}$$

$$\mathbf{u}_i^{n+1}(x^{(n+1)}_{i+\frac{1}{2}} - x^{(n+1)}_{i-\frac{1}{2}}) = \frac{1}{2}\mathbf{u}_i^n(x^n_{i+\frac{1}{2}} - x^n_{i-\frac{1}{2}}) + \frac{1}{2}\mathbf{u}_i^{(1)}(x^{(1)}_{i+\frac{1}{2}} - x^{(1)}_{i-\frac{1}{2}}) + \frac{1}{2}\Delta t \mathcal{R}(\mathbf{u}^{(1)}) \tag{12}$$

# 4 The Linearised Riemann Solver

In 1D, the Linearised Riemann Solver [4] is used to determine the flux as

$$\mathbf{f}(\mathbf{u}_L, \mathbf{u}_R) = \frac{1}{2}(\mathbf{f}(\mathbf{u}_L) + \mathbf{f}(\mathbf{u}_R) - \dot{x}(\mathbf{u}_L + \mathbf{u}_R)) - \frac{1}{2}\mathbf{R}|\Lambda|\mathbf{L}(\mathbf{u}_R - \mathbf{u}_L) \tag{13}$$

where

$$\mathbf{R} = \left[\begin{array}{c|c|c} 1 & 1 & 1 \\ u-a & u & u+a \\ H-ua & \frac{1}{2}u^2 & H+ua \end{array}\right] \tag{14}$$

$$\mathbf{L} = \frac{1}{2a^2}\left[\begin{array}{c|c|c} \frac{\gamma-1}{2}u^2 + ua & -(\gamma-1)u - a & (\gamma-1) \\ 2a^2 - (\gamma-1)u^2 & 2(\gamma-1)u & -2(\gamma-1) \\ \frac{\gamma-1}{2}u^2 - ua & -(\gamma-1)u + a & (\gamma-1) \end{array}\right]. \tag{15}$$

and $\Lambda = \mathrm{diag}(u - a - dotx, u - \dot{x}, u + a - \dot{x})$ with $a$ and $u$ as density-averaged variables from $\rho = \sqrt{\rho_L \rho_R}$ and

$$u = \frac{\sqrt{\rho_L}u_L + \sqrt{\rho_R}u_R}{\sqrt{\rho_L} + \sqrt{\rho_R}} \qquad H = \frac{\sqrt{\rho_L}H_L + \sqrt{\rho_R}H_R}{\sqrt{\rho_L} + \sqrt{\rho_R}} \qquad a = \sqrt{(\gamma-1)\left(H - \frac{1}{2}u^2\right)} \tag{16}$$

In the pure Lagrangian case, the mass is assumed constant in each cell, and the flux is then

$$\mathbf{f} - u\mathbf{u} = \left[\begin{array}{c} 0 \\ p \\ up \end{array}\right] \tag{17}$$

with an alternative choice of $u$ as $u = \frac{1}{2}(u_L + u_R) - \frac{(p_R - p_L)}{2\rho a}$ and with $p = \frac{1}{2}(p_L + p_R) - \frac{1}{2}\rho a(u_R - u_L)$.

## 4.1 On consistency? of the Solver

We observe that in the pure lagrangian case, the mass flux

$$(\mathbf{f} - u\mathbf{u})_1 \neq 0 \tag{18}$$

but that, in the choice of $u = \frac{\sqrt{\rho_L}u_L + \sqrt{\rho_R}u_R}{\sqrt{\rho_L} + \sqrt{\rho_R}}$

$$\begin{aligned}
(\mathbf{f} - u\mathbf{u})_1 &= \frac{1}{2}(\rho_L u_L + \rho_R u_R - u(\rho_L + \rho_R) - \Delta p/a) && (19)\\
&= \frac{1}{2}(\rho_L(u_L - u) + \rho_R(u_R - u) - \Delta p/a) && (20)\\
&= \frac{1}{2}\left(\sqrt{\rho_L\rho_R}\left(\frac{\sqrt{\rho_R} - \sqrt{\rho_L}}{\sqrt{\rho_R} + \sqrt{\rho_L}}\right)\Delta u - \frac{\Delta p}{a}\right) && (21)\\
&= \frac{1}{2}\left(\left(\frac{\sqrt{\rho_L\rho_R}}{(\sqrt{\rho_R} + \sqrt{\rho_L})^2}\right)\Delta\rho\Delta u - \frac{\Delta p}{a}\right) && (22)
\end{aligned}$$

# 5 Dukowicz's two-shock Riemann scheme (DKWZ) [5]

For $i = L, R$

$$p - p_i = \rho_i[a_i + A_i|u - u_i|](u - u_i) \tag{23}$$

and for an ideal gas, $a_i = \sqrt{\frac{\gamma p_i}{\rho_i}}$ and $A_i = \lim_{\text{strongshock}}[(\rho_2/\rho_1)/(\rho_2/\rho_1 - 1)] = \frac{1}{2}(\gamma + 1)$. This results in two equations and two unknowns which can be solved for. These equations are

$$p_R - p_L + \rho_R(a_R + A|u - u_R|)(u - u_R) - \rho_L(a_L + A|u - u_L|)(u - u_L) = 0 \tag{24}$$

$$p = \frac{1}{2}(p_L + p_R) + \frac{1}{2}(\rho_R(a_R + A|u - u_R|)(u - u_R) - \rho_L(a_L + A|u - u_L|)(u - u_L)) \tag{25}$$

# 6 Sod's Problem

Sod's problem [6] is a shocktube with $[\rho, u, p]_L = [1.0, 0.0, 1.0]$ and $[\rho, u, p]_R = [0.125, 0.0, 0.1]$. I use this problem partly because it is used in [7], which is a terrible paper, but nonetheless is some of the only material on this subject and gives me something to compare to. Here are some simple results, all done on an initially uniform grid with 400 cells with a CFL number of 0.8 and using the both timestepping schemes. All results are second order with a harmonic limiter applied to slopes.

Results for Roe's Riemann Solver can be seen in Figures 3 and 4. Results for Dukowicz's Riemann Solver can be seen in Figures 5 and 6. Results for the Exact Riemann Solver can be seen in Figures 7 and 8. A brief comparison of all the results for the Hancock scheme are seen in Figure 2.

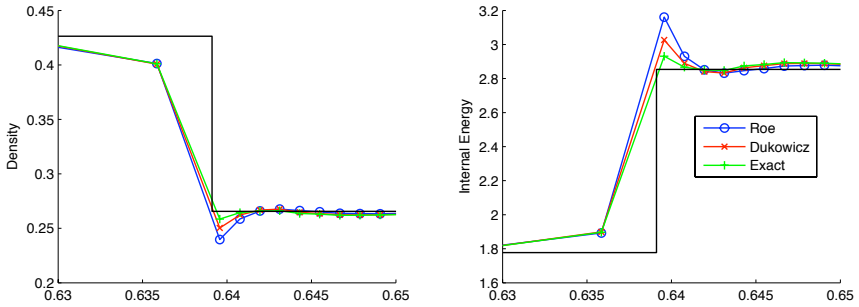


Figure 2: Contact Discontinuity area using Roe, Dukowicz, and Exact Lagrangian Riemann Solvers

## 6.1 Examination of the Dukowicz Riemann Solver

In the Dukowicz Riemann Solver, we have

$$A_i = \lim_{\text{strongshock}}[(\rho_2/\rho_1)/(\rho_2/\rho_1 - 1)] = \frac{1}{2}(\gamma + 1) \tag{26}$$

I can adjust it for the weak limit by defining a constant $C$ and letting

$$A_i = C\frac{1}{2}(\gamma + 1) \qquad C > 1 \tag{27}$$

Here results are shown with the Hancock scheme. Looking at the results in Figures 9 and 10, adjusting this parameter improves things slightly, as expected.

# 7 Lax Problem

Lax's problem is a shocktube with $[\rho, u, p]_L = [0.445, 0.698, 3.528]$ and $[\rho, u, p]_R = [0.5, 0, 0.571]$. Here, similar to the work of Cheng and Shu [8], 100 uniform cells are used. Again, results shown in Figure 11 are at $t = 0.01$ and done with CFL number of 0.8. All three Lagrangian Riemann Solvers perform equally well.

# 8 Woodward and Colella Double Blast Wave

Here the Woodward and Colella double blast wave problem [9] is examined. The initial data is for $x \in [0, 1]$ with

$$\rho = 1, \qquad u = 1, \qquad p = \begin{cases} 10^3 & x \leq 0.1 \\ 10^{-2} & 0.1 < x < 0.9 \\ 10^2 & 0.9 \leq x \end{cases} \tag{28}$$

and reflecting boundary conditions. This problem is notoriously tough due to its strong shocks. Results shown in Figure 12 are at $t = 0.038$ and done with CFL number of 0.5. There are initially 200 uniformly spaced cells. All three Lagrangian Riemann Solvers perform equally well.

# 9 Leblanc Problem

The Leblanc problem consists of $x \in [0, 9]$ and

$$[\rho, u, i] = \begin{cases} 1, 0, 0.1 & x < 3 \\ 0.001, 0, 10^{-7} & x > 3 \end{cases} \tag{29}$$

with $\gamma = 5/3$.

# 10 The Slowly Moving Shock Problem

Here we take a problem similar to that by Arora and Roe [10] with $[\rho, u, p]_L = [3.86, -0.81, 10.33]$ and $[\rho, u, p]_R = [1, -3.44, 1]$

# 11 Euler Equations in Lagrangian Coordinates [11]

Here we have equations in mass coordinates as

$$\mathbf{u}_t + \mathbf{f}(\mathbf{u})_m = 0 \tag{30}$$

with

$$\frac{\partial}{\partial t}\begin{bmatrix} V \\ u \\ E \end{bmatrix} + \frac{\partial}{\partial m}\begin{bmatrix} -u \\ p \\ up \end{bmatrix} = \begin{bmatrix} 0 \\ 0 \\ 0 \end{bmatrix}, \tag{31}$$

For $V = \frac{1}{\rho}$ and $E = i + \frac{1}{2}u^2$. Here, we have three wave speeds $\lambda = [-A, 0, A]$ with $A = a/V = \sqrt{\frac{\gamma p}{V}}$ for a Lagrangian sound speed $A$ and $p = (\gamma - 1)\frac{i}{V}$. The Linearised Riemann solver flux is

$$\mathbf{f}(\mathbf{u}_L, \mathbf{u}_R) = \frac{1}{2}(\mathbf{f}_L + \mathbf{f}_R) - \frac{1}{2}\mathbf{R}|\Lambda|\mathbf{L}(\mathbf{u}_R - \mathbf{u}_L) \tag{32}$$

for

$$\mathbf{R} = \left[\begin{array}{c|c|c} 1 & 1 & 1 \\ A & 0 & A \\ uA - p & \frac{p}{\gamma - 1} & -uA - p \end{array}\right] \tag{33}$$

$$\mathbf{L}(\mathbf{u}_R - \mathbf{u}_L) = \begin{bmatrix} \frac{1}{2A}\left(\frac{\Delta p}{A} - \Delta u\right) \\ -\Delta V - \frac{\Delta p}{A^2} \\ \frac{1}{2A}\left(\frac{\Delta p}{A} + \Delta u\right) \end{bmatrix} \tag{34}$$

and mean values

$$V = \frac{1}{2}(V_R + V_L) \qquad u = \frac{1}{2}(u_R + u_L) \qquad p = \frac{1}{2}(p_R + p_L) \qquad A = \sqrt{\frac{\gamma p}{V}} \tag{35}$$

Mapping between mass and spatial coordinates can be done with

$$\Delta m_i = \rho_i \Delta x_i \quad \rightarrow \quad x_j = \sum_{i=1}^{j} V_i \Delta m_i \tag{36}$$

## 11.1 Munz's Timestepping Scheme

He uses a funny scheme.

$$\mathbf{u}^n_{i\pm} = \mathbf{u}_i \pm \frac{\Delta m_i}{2}\mathbf{S}^n_i \tag{37}$$

To get slopes, he calculates

$$\overline{\mathbf{u}}^n_i = \frac{1}{4}(\mathbf{u}^n_{i+1} + 2\mathbf{u}^n_i + \mathbf{u}^n_{i-1}) \tag{38}$$

and determines the Jacobian $\mathbf{A}(\overline{\mathbf{u}}^n_i)$. Now solve for

$$\frac{2}{\Delta m_{i+1} + \Delta m_i}(\mathbf{u}^n_{i+1} - \mathbf{u}^n_i) = \sum_k \alpha^k_i \mathbf{r}^k_i, \qquad \frac{2}{\Delta m_i + \Delta m_{i-1}}(\mathbf{u}^n_i - \mathbf{u}^n_{i-1}) = \sum_k \beta^k_i \mathbf{r}^k_i \tag{39}$$

Finally, solve for the slopes as

$$\mathbf{S}^n_i = \sum_k s(\alpha^k_i, \beta^k_i)\mathbf{r}^k_i \tag{40}$$

Otherwise, it is the same as our hancock.

# References


[1] Zaide, D. W. and Roe, P. L., "Entropy-based Mesh Refinement, II: A New Approach to Mesh Movement, AIAA paper, 19th AIAA CFD Meeting, San Antonio, 2009," .

[2] Berthon, C., "Why the MUSCL-Hancock scheme is L1 -stable," *Numerische Mathematik*, Vol. 104, 2006, pp. 27–46.

[3] Suzuki, Y., *Discontinuous Galerkin methods for extended hydrodynamics*, Ph.D. thesis, University of Michigan, 2008.

[4] Roe, P. L., "Approximate Riemann Solvers, Parameter Vectors and Difference Schemes," *J. Comput. Phys.*, Vol. 43, 1981, pp. 357–372.

[5] Dukowicz, J., "A general, non-iterative Riemann solver for Godunov's method," *Journal of computational physics(Print)*, Vol. 61, No. 1, 1985, pp. 119–137.

[6] Sod, G., "A survey of several difference methods for hyperbolic systems of nonlinear conservation laws," *J. Comput. Phys.*, Vol. 27, 1978, pp. 1–31.

[7] Tian, B., Shen, W., Jiang, S., Wang, S., and Liu, Y., "An arbitrary Lagrangian-Eulerian method based on the adaptive Riemann solvers for general equations of state," *International Journal for Numerical Methods in Fluids*, Vol. 59, No. 11, 2009.

[8] Cheng, J. and Shu, C., "A high order ENO conservative Lagrangian type scheme for the compressible Euler equations," *Journal of Computational Physics*, 2007.

[9] Woodward, P. and Colella, P., "The Numerical Simulation of Two-Dimensional Fluid Flow with Strong Shocks," *J. Comput. Phys.*, Vol. 54, 1984, pp. 115–173.

[10] Arora, M. and Roe, P., "On postshock oscillations due to shock capturing schemes in unsteady flows," *Journal of Computational Physics*, Vol. 130, No. 1, 1997, pp. 25–40.

[11] Munz, C., "On Godunov-type schemes for Lagrangian gas dynamics," *SIAM Journal on Numerical Analysis*, 1994, pp. 17–42.

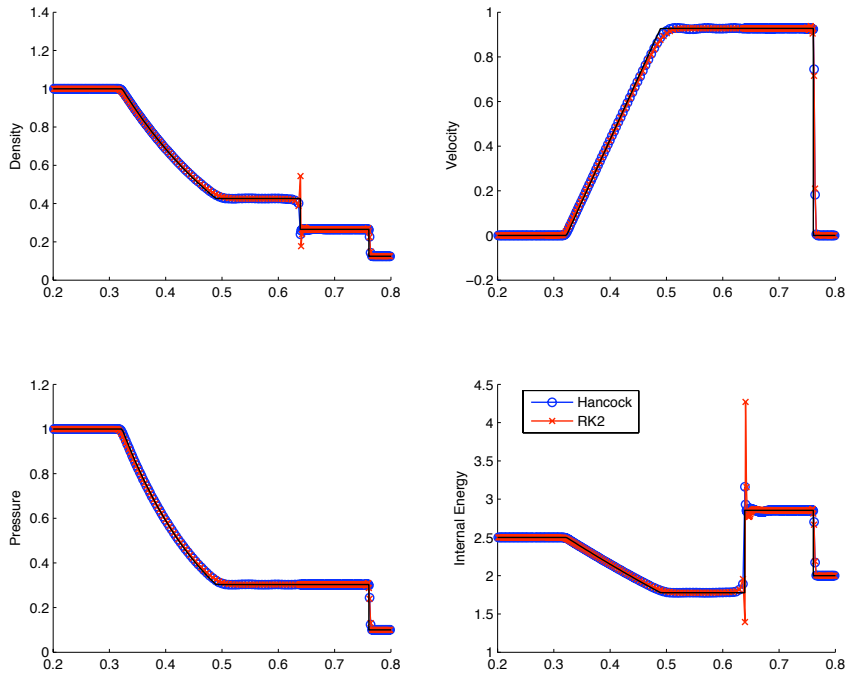


Figure 3: Density, Velocity, Pressure, and Internal Energy for Roe's Riemann Solver.

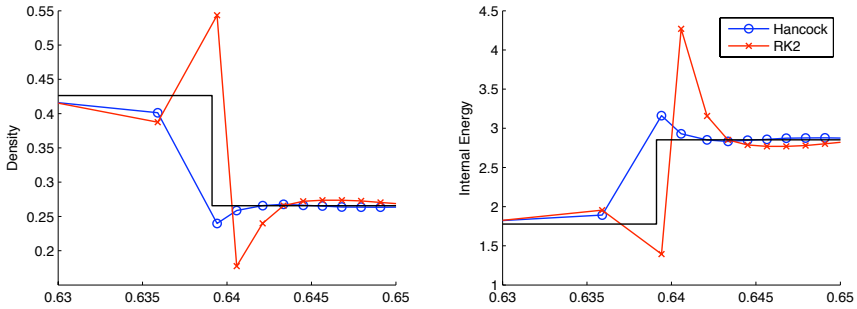


Figure 4: Same as above, but zoomed in around the contact.

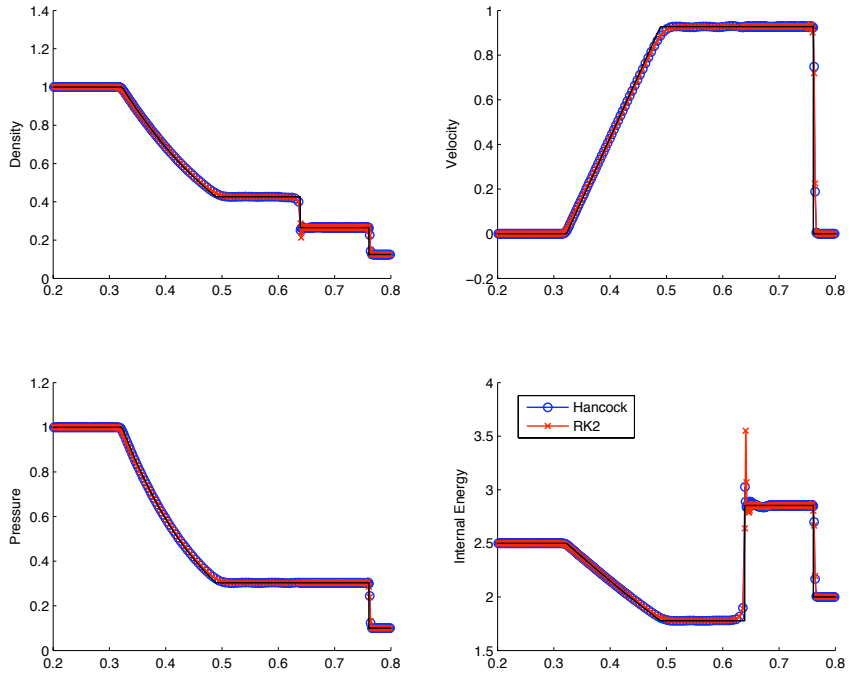


Figure 5: Density, Velocity, Pressure, and Internal Energy for Dukowicz's Riemann Solver.

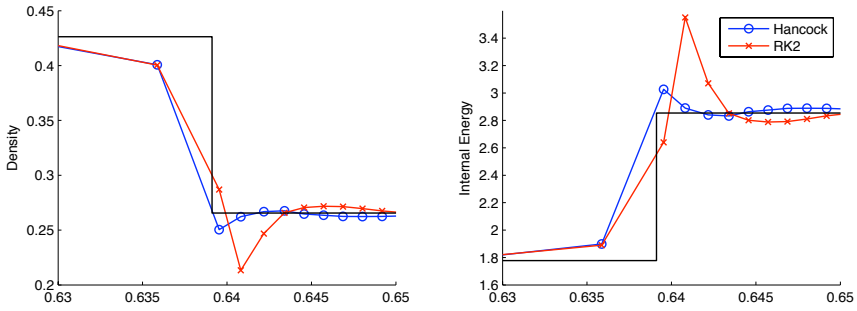


Figure 6: Same as above, but zoomed in around the contact.

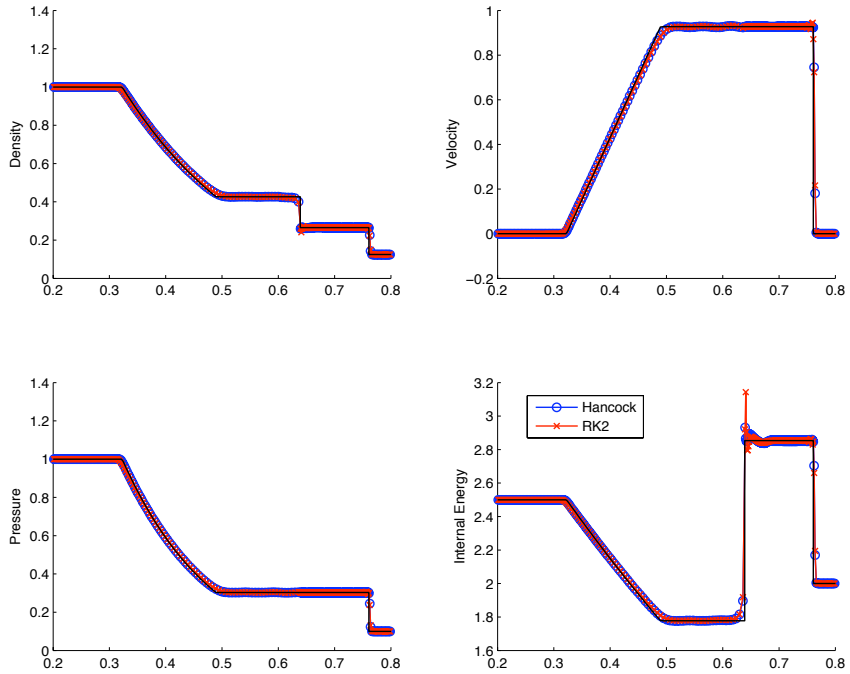


Figure 7: Density, Velocity, Pressure, and Internal Energy for the Exact Riemann Solver.

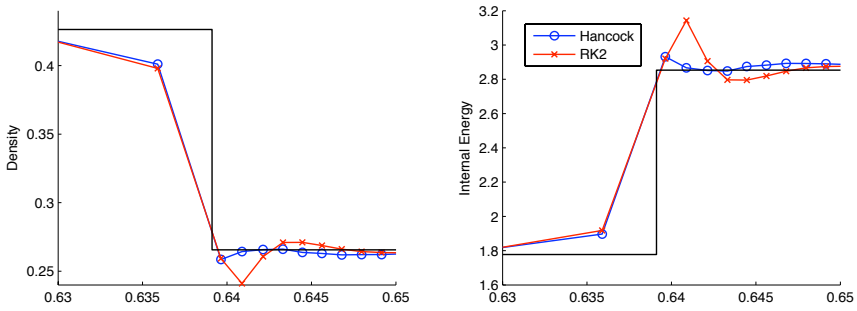


Figure 8: Same as above, but zoomed in around the contact.

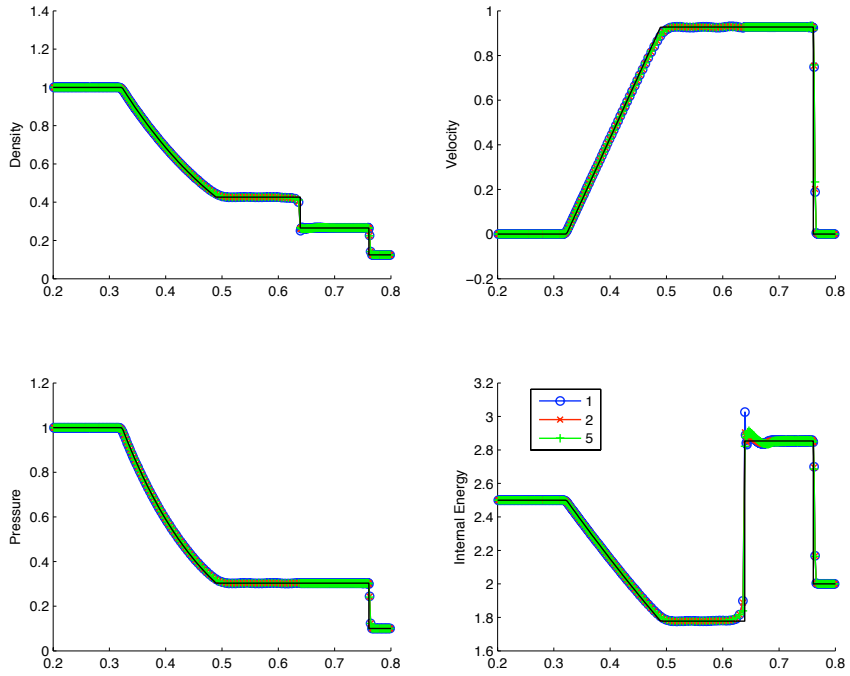


Figure 9: Effect of Modifying $A_i$ in the Dukowicz Riemann Solver by a constant $C$ for $C = 1$, blue $\circ$, $C = 2$, red $\times$, and $C = 5$, green $+$.

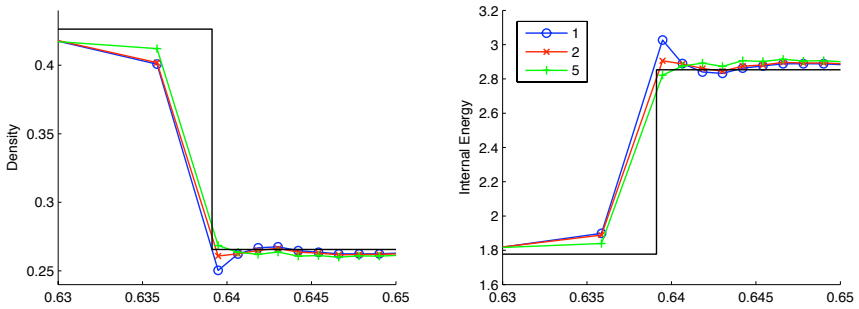


Figure 10: Same as above, but zoomed in around the contact.

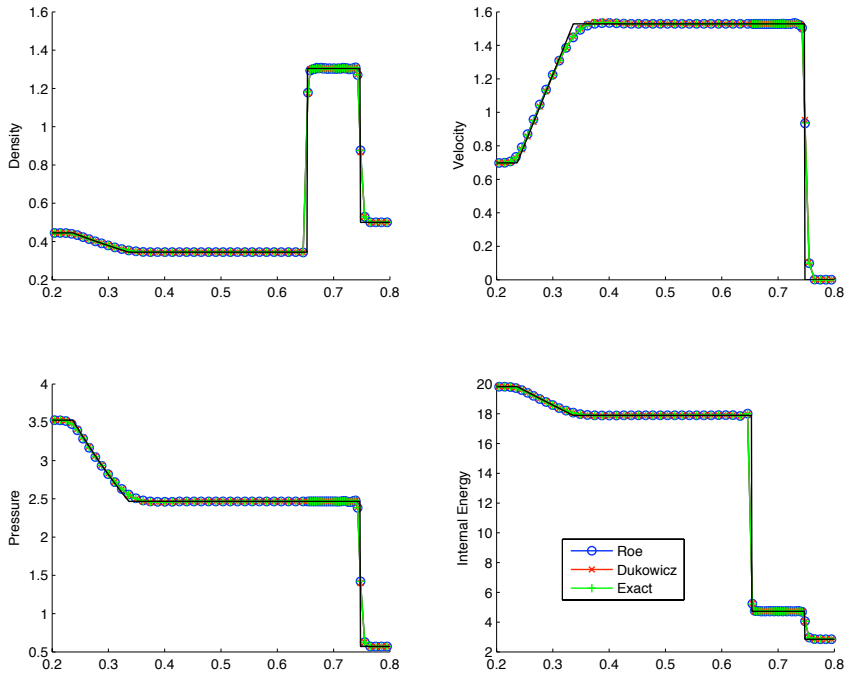


Figure 11: Lax Problem using Roe, Dukowicz, and Exact Lagrangian Riemann Solvers

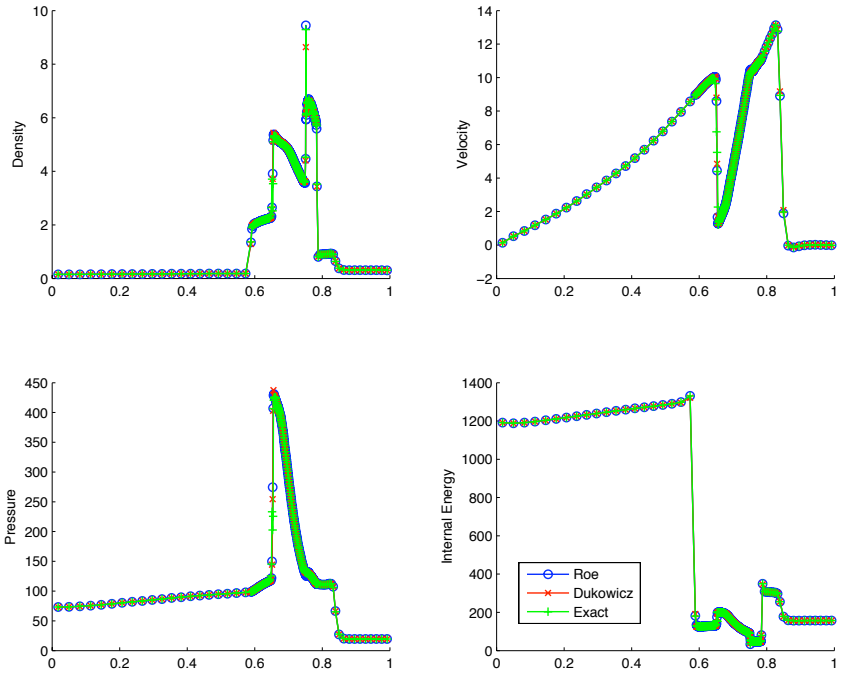


Figure 12: Woodward-Colella Problem using Roe, Dukowicz, and Exact Lagrangian Riemann Solvers